Robust Simultaneous Localization and Mapping Using the Relative Pose Estimation of Trilateration UHF RFID Tags

Emidio Di Giampaolo, Francesco Martinelli, and Fabrizio Romanelli

***Abstract*—We consider a mobile robot equipped with wheel encoders and a RFID reader, which measures the phase of the signal backscattered by a set of passive UHF-RFID tags, deployed in unknown position on the ceiling of the environment. We deal with a Simultaneous Localization And Mapping (SLAM) problem, where the position of the tags must be estimated to create a reference map, within which the robot will be localized. One of the contributions of the paper is the use of a special kind of tag, the TriLateration Tag (TLT), including three antennas close one each other. The solution is based on the range and bearing estimation of all TLT detected, performed through a set of Multi-Hypothesis Extended Kalman Filters (MHEKF), one for each TLT. Then, the range and the bearing information of the responding TLTs is used in an EKF-SLAM algorithm which solves the SLAM problem. The proposed approach is more robust and computationally efficient with respect to other approaches available in the literature and is particularly suited for large warehouses where RFID tags cannot be deployed too densely.**

***Index Terms*—RFID localization, robust Kalman filtering, UHF-RFID, SLAM, resilient sensor fusion.**

I. Introduction

RFID technology for robot localization is becoming widespread in several contexts: in fact, off-the-shelf passive RFID systems allow to develop low cost, low invasive, maintenance free localization structures, which may work in harsh environments not suitable to other kinds of sensors. Moreover, the knowledge of the ID of the responding RFID tags allows to bypass the data association problem, afflicting other kinds of sensors.

Several methods have been presented in the literature in this context: a comprehensive survey on this subject has been recently presented in [1], where it is observed that the most investigated and relevant approach in this framework is the one where phase measurements (i.e., the phase shift in the signal backscattered by RFID tags) are combined with proprioceptive sensors. This is actually also the context considered in this paper, where a reader, installed on board a mobile robot, measures the phase shift in the signal coming from a set of passive UHF-RFID tags deployed in unknown position on the ceiling of the environment.

One of the main problems with phase measurements is their cyclicality, since a given phase shift corresponds to several possible tag-reader distances. A vast literature has faced this problem (see, e.g., [2], [3], [4], [5], [6]). One possibility in the robot localization framework is to adopt multi-hypotheses filters where wrong hypotheses (e.g., on the robot pose, like in [7]) are pruned according to the phase measurements which become available during the reader (or the tag) motion.

Many approaches (e.g., [7], [8], [9], [10]) rely on the assumption that the position of the tags is known, while in practice, also due to technological reasons (like the uncertainty in the antenna phase center [11]), this can not be guaranteed, even because a precise knowledge of the position of the tags is needed in view of the high sensitivity of the phase measurements.

It is relevant, for this reason, to develop approaches where also the tag positions, together possibly with other unknown parameters (like the offset in the phase measurements), are included in the estimation algorithm, as done, e.g., in [12] and [13], where, however, an approximate guess on these quantities is assumed available at the beginning. If, on the contrary, the position of the tags (and the phase offset) is completely unknown, a Simultaneous Localization and Mapping (SLAM) problem arises.

To the best of the authors knowledge, solutions to the SLAM problem based exclusively on RFID phases as external measurements are quite missing in the literature, where other kinds of measurements (like, e.g., RSSI [14] or time of flight [15]) are usually assumed available. In some cases (see, e.g., among the others, [16]), the SLAM is solved resorting to other technologies and, only once the robot is localized, phase measurements are used to map tagged objects in the created map. In our case, on the contrary, SLAM is the main problem addressed and we want to solve it only using RFID phases as external measurements.

Now, since phases represent an ambiguous measurement of the tag-reader distance, the problem is actually a variant (with increased difficulty, due to the ambiguity) of a Range-Only SLAM (RO-SLAM) problem, where the information on the

Manuscript received 29 April 2022; accepted 24 May 2022. Date of publication 2 June 2022; date of current version 23 September 2022. This work was supported in part by the Italian Ministry for Research in the framework of the Program for Research Projects of National Interest (PRIN) under Grant 2017YKXYXJ and Grant 2020RTWES4. *(Corresponding author: Francesco Martinelli.)*

Emidio Di Giampaolo is with the Department of Industrial and Information Engineering and Economics, University of L'Aquila, 67100 L'Aquila, Italy (e-mail: emidio.digiampaolo@univaq.it).

Francesco Martinelli and Fabrizio Romanelli are with the Department of Civil Engineering and Computer Science, University of Rome Tor Vergata, 00133 Rome, Italy (e-mail: francesco.martinelli@uniroma2.it; fabrizio.romanelli@uniroma2.it).

Digital Object Identifier 10.1109/JRFID.2022.3179045

bearing of the responding tag is missing from the available measurements. For this reason, one possible way to solve the problem, described in [17], extends the RO-SLAM technique proposed in [18] to consider the phase periodicity. It provides a satisfactory solution, where also the offset of the tags is handled as part of the estimation of the ceiling height (where tags are placed), which is assumed only roughly known at the beginning.

Two major limits afflict, however, the algorithm proposed in [17]: the computational complexity, large at the beginning due to the large number of candidate EKF instances associated with each new observed tag and the non negligible possibility of failures. In order to comply with this second issue, a restarting paradigm for the filter was proposed in [19] to reinitialize the robot pose estimation in case of filter divergence. However, this method works only if the divergence of the filter is caused by a wrong estimate of the robot position and does not reduce the computational complexity of the original algorithm. The approach in [19] could be improved by designing a diagnostic module able to understand which is the cause of the filter divergence (if a failure in the robot or in the tags estimates). This task, however, is not simple, especially under low densities of RFID tags (which is the case considered in our setting).

Due to these reasons, a different solution approach was proposed in [20]. It exploits the Multi Hypothesis Extended Kalman Filter (MHEKF) developed in [21] which, based on the wheel encoder readings and on the phase measurements coming from a given tag, is able to provide an estimate of the range and of the bearing of that tag with respect to the robot. Once the range and the bearing of the tags is available, given that the ID of the tags is known, an EKF-SLAM based algorithm can be successfully adopted to solve the problem.

The proposed approach presents a time complexity quite lower with respect to the approach proposed in [17]. In fact, even if there is a MHEKF running for each tag, every MHEKF contains a limited number of EKF instances (typically between 10 or 20, depending on the maximum detection range) and each instance is a three dimensional EKF (it estimates the range, the bearing and the phase offset of the tag).

Another interesting feature of the proposed approach is the robustness against disturbances, since, in this case, unlike in [17], hypotheses are not pruned and the algorithm may be able to restore a good behavior after possible unmodeled perturbations.

This paper extends [20] by replacing standard RFID tags with structures (denoted in the following as *TriLateration Tags (TLT)*) comprising three tag antennas close one each other. This kind of RFID tags, already investigated in [22] in a pure localization context (i.e., where the position of the tags and the offsets are assumed known at the beginning), allows to obtain, under negligible additional costs and installation work, a solution which improves the performance with respect to the case standard tags are considered, without a significant increase in the computational complexity of the algorithm. As shown in the paper, the steady state localization error is significantly lower than the one obtained with uniform mesh of standard tags, deployed with the same density and in principle, if also the orientation of the TLT is considered in the SLAM algorithm, it would be possible to solve a SLAM problem even if only one of these TLT is available. For all these reasons, the proposed approach is particular appealing in large environments, such as warehouses, where tags should be deployed with very low densities. A numerical and an experimental analysis of the behavior of the proposed algorithm in noisy environments, characterized by a non negligible level of multipath, is reported in this paper as an additional contribution with respect to [20]. According to this analysis, it is possible to conclude that the proposed solution presents a certain degree of robustness also with respect to this kind of phenomena.

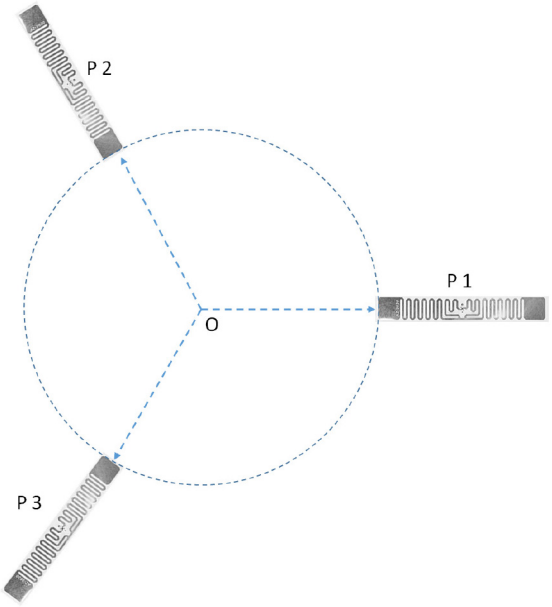

Fig. 1. Schema of the TriLateration Tag (TLT) with the three antennas located in points P_i, $i = 1, 2, 3$, at a mutual distance of the order of 10 cm.

II. Notation and Problem Formulation

We consider an indoor environment with L RFID TriLateration Tags located on the ceiling. Each TLT is a structure of the type reported in Fig. 1. The ceiling height will be denoted by h and will be assumed known. The robot is a unicycle-like vehicle with a differential drive kinematics. If $(x_{r,t}, y_{r,t}, \theta_t)$ denotes the robot pose at time t, with $(x_{r,t}, y_{r,t})$ the robot position and θ_t its orientation, the robot discrete time dynamics is:

$$\begin{bmatrix} x_{r,k+1} \\ y_{r,k+1} \\ \theta_{k+1} \end{bmatrix} = \begin{bmatrix} x_{r,k} + u_k \cos(\theta_k) \\ y_{r,k} + u_k \sin(\theta_k) \\ \theta_k + \omega_k \end{bmatrix}, \tag{1}$$

where $u_k = \frac{u_{R,k}+u_{L,k}}{2}$ and $\omega_k = \frac{u_{R,k}-u_{L,k}}{d}$, being $u_{R,k}$ and $u_{L,k}$ the distance covered in the time interval $(k\delta_t, (k+1)\delta_t)$ (i.e., at time step k, with discretization step δ_t) by the right and the left wheel, respectively and d the distance between the two wheels. The distance $u_{R,k}$ covered at time step k by the right wheel is related to a noisy encoder reading $u^e_{R,k}$ by the relation $u^e_{R,k} = u_{R,k} + n_{R,k}$, where the noise term $n_{R,k}$ is assumed

a 0-mean Gaussian random variable with variance given by $K_R|u^e_{R,k}|$, being K_R a positive constant. A similar argument can be applied to the left wheel. Accordingly, we define also $u^e_k = \frac{u^e_{R,k}+u^e_{L,k}}{2}$ and $\omega^e_k = \frac{u^e_{R,k}-u^e_{L,k}}{d}$.

A reader installed onboard the robot collects the phases of the RFID signals backscattered by L TLTs located in unknown positions $(x_{T_1}, y_{T_1}), \ldots, (x_{T_L}, y_{T_L})$. The phase measurement at time k collected by the reader onboard the robot for each tag in the TLTs can be defined as:

$$\phi_k = \mod\left(-2KD_k + \phi_o + \phi_{m,k} + n_{\phi,k}, 2\pi\right), \tag{2}$$

where $K = 2\pi/\lambda$ (with λ the wavelength of the electromagnetic signal, $\lambda = 34.6cm$ in our tests), D_k is the (unknown) tag-reader distance, ϕ_o is an unknown offset depending on the hardware, $n_{\phi,k}$ is, at each time k, a 0-mean Gaussian noise with standard deviation σ_ϕ and $\phi_{m,k}$ is a disturb of the phase that accounts for effects (i.e., multipath) of the environment. It is assumed that the tags can be detected only if their distance from the robot is less than a threshold: namely a tag can be detected when the robot lies in a circle of radius ρ_M centered on the projection of the tag on the floor.

The problem considered in this paper is a Simultaneous Localization and Mapping (SLAM) problem, where both the robot pose and the tags position must be estimated at the same time.

III. Solution Approach

The solution approach is based on the estimation of the range and the bearing of each TLT with respect to the robot (see Section III-A), which is then used in an EKF-SLAM algorithm (see Section III-B).

A. TriLateration Tag Range and Bearing Estimation

The case of tags comprising a single antenna was considered in [21]. When the robot moves, the range and the bearing of any single antenna tag change over time. As described in [21], knowing the wheel displacements $u_{R,k}$ and $u_{L,k}$, it is possible to derive the equations which describe the dynamics of the range and the bearing of a given tag and to define a Multi-Hypothesis Extended Kalman Filter (MHEKF), that fuses the phase measurements with the odometry readings to obtain an estimate of these quantities. The MHEKF consists of a set of EKF instances initialized on the different cycles associated with the first phase measurement arrived from the tag. The instance with the largest weight (i.e., with the largest agreement with the available measurements) is selected to provide the range and the bearing estimate of the tag with respect to the robot (see [21] for more details).

Now consider the case of TriLateration Tags. We could clearly proceed by independently estimating the range and the bearing of the three antennas forming the TLT, applying the procedure just discussed. However, since we know the relative distance between the three antennas forming the TLT, we can consider a more effective approach, where the TLT is regarded to as a triangular structure (with known shape and size) and we want to estimate the relative pose of this structure with respect to the robot.

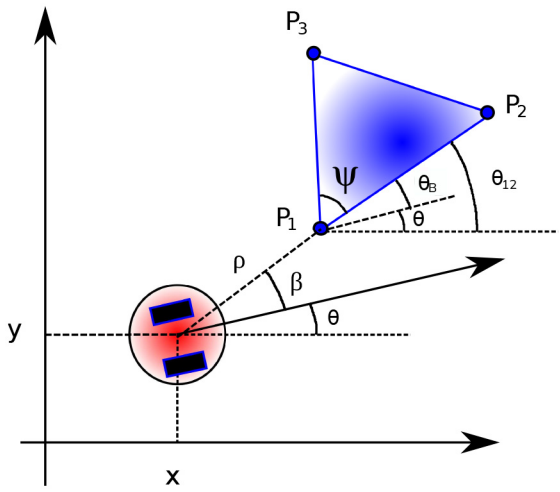

Fig. 2. Geometric description of a TLT.

So, if i and j, $i, j \in \{1, 2, 3\}$, are two antennas in the TLT, let L_{ij} be the known distance between antennas i and j.

Let $P_1 = (x_1^{TLT}, y_1^{TLT})$, $P_2 = (x_2^{TLT}, y_2^{TLT})$ and $P_3 = (x_3^{TLT}, y_3^{TLT})$ be the vertexes of the triangle formed by the three antennas of the TLT (see Fig. 2). We will consider as reference point in the TLT the vertex P_1, and, at time step k, we will define the range and the bearing of the TLT by considering the range ρ_k and the bearing β_k of this vertex with respect to the robot:

$$\rho_k = \sqrt{\left(x_1^{TLT} - x_{r,k}\right)^2 + \left(y_1^{TLT} - y_{r,k}\right)^2}, \tag{3}$$

$$\beta_k = \text{atan2}\left(y_1^{TLT} - y_{r,k}, x_1^{TLT} - x_{r,k}\right) - \theta_k. \tag{4}$$

We now introduce also the angle θ_B between the line through P_1 and P_2 and the robot orientation:

$$\theta_{B,k} = \theta_{12} - \theta_k, \tag{5}$$

where $\theta_{12} = \text{atan2}(y_2^{TLT} - y_1^{TLT}, x_2^{TLT} - x_1^{TLT})$ is the constant (unknown) angle between the line through P_1 and P_2 and the x-axis of the global reference frame.

It is possible to derive the discrete time dynamics of these quantities (in particular the dynamics of ρ and β has been presented in [21], while the third is straightforward) to obtain:

$$\rho_{k+1} = \rho_k - u_k \cos(\beta_k), \tag{6}$$

$$\beta_{k+1} = \beta_k + \frac{u_k}{\rho_k}\sin(\beta_k) - \omega_k, \tag{7}$$

$$\theta_{B,k+1} = \theta_{B,k} - \omega_k. \tag{8}$$

The available measurements are the phase readings from the three antennas forming the TLT. To write these measurements, we first compute the distance D_1, D_2 and D_3 of, respectively, antennas 1, 2 and 3 of the TLT from the robot. Exploiting the TLT variables defined so far, we can write:

$$D_1 = \sqrt{\rho^2 + h^2}, \tag{9}$$

$$D_2 = \sqrt{\rho^2 + L_{12}^2 + 2\,\rho\,L_{12}\cos(\beta - \theta_B) + h^2} \tag{10}$$

$$D_3 = \sqrt{\rho^2 + L_{13}^2 + 2\,\rho\,L_{13}\cos(\beta - \theta_B - \psi) + h^2}, \tag{11}$$

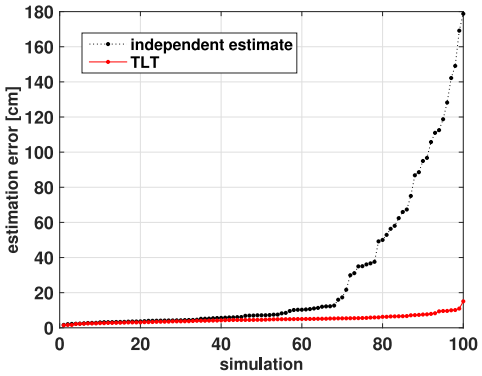

Fig. 3. Average position estimation error of the three antennas in the TLT performed by the 3D MHEKF proposed in this paper and by independently estimating these positions through three 2D MHEKF as the ones in [20].

where ψ is the (constant and known) angle between the line through P_1 and P_2 and the line through P_1 and P_3 (see Fig. 2). The phase measurements from the three antennas forming the TLT can then be written as in (2), with D_k respectively given by (9), (10) and (11).

It is possible to estimate the pose of the TLT with respect to the robot, i.e., to estimate the variables (ρ, β, θ_B) through a MHEKF applied to the system with dynamics (6)-(8) and using the phase measurements coming from the three antennas of the TLT. The detailed steps of the MHEKF are reported in Algorithm 1.

The proposed solution outperforms the approach where the range and the bearing of the three antennas were estimated independently both in performance and also in computational time, since only one 3D MHEKF per TLT is necessary in place of three 2D MHEKF, one for each antenna. In the average, the time needed to execute the 3D MHEKF for each TLT is less than half the time needed by three independent 2D MHEKF.

As for the performance, to compare the two approaches we have executed 100 independent simulations. We have assumed a standard deviation $\sigma_\phi = 10°$ on the error in the phase measurements, with the three antennas in the TLT positioned in (120, 120), (130, 125) and (120, 130) cm. The robot performs random paths of 1000 steps under the TLT, which is located on the ceiling at a height $h = 255$ cm. Other parameters are like in Section IV. In each simulation we have computed an average steady state estimation error on the position of the three antennas in the TLT by considering the estimation error in the last 200 steps of each simulation. These errors are reported in Fig. 3: it is possible to observe how the proposed approach provides a significant improvement with respect to the independent version of [20].

As in [20], the offset of the three antennas in the TLT can be included in the estimation process, as done in the experimental test of Section V, by considering a 6D MEKF (it was 3D in [20]). The estimation of the offset may also compensate an uncertainty in the knowledge of the ceiling height and other unmodeled phenomena, as discussed in Section V.

Algorithm 1 The Multi-Hypothesis Extended Kalman Filter (MHEKF) for range and bearing estimation of TLTs

Initialization. Let n_M be an integer defining the number of EKF instances and let $\Delta_\rho = \rho_M / n_M$ be the range interval differentiating the instances at the beginning (n_M should be selected not smaller than the number of possible ranges corresponding to a phase measurement). Initialize n_M EKF instances $\ell = 0, 1, \ldots, n_M - 1$ with an initial estimate and covariance matrix given by

$$\hat{\rho}_0^\ell = \Delta_\rho/2 + \ell \cdot \Delta_\rho, \tag{12}$$

$$\hat{\beta}_0^\ell = 0, \tag{13}$$

$$\hat{\theta}_{B,0}^\ell = 0, \tag{14}$$

$$P_0^\ell = \begin{bmatrix} \Delta_\rho^2/12 & 0 & 0 \\ 0 & (\pi/3)^2 & 0 \\ 0 & 0 & (\pi/3)^2 \end{bmatrix}. \tag{15}$$

Initialize the time step by assigning $k = 0$.

Prediction step. At each time step k, independently in each EKF instance ℓ, compute the a priori estimates based on Eqs. (6)-(8):

$$\hat{\rho}_{k+1}^{\ell,-} = \hat{\rho}_k^\ell - u_k^e \cos(\hat{\beta}_k^\ell), \tag{16}$$

$$\hat{\beta}_{k+1}^{\ell,-} = \hat{\beta}_k^\ell + \omega_k^e + \frac{u_k^e}{\hat{\rho}_k^\ell} \sin(\hat{\beta}_k^\ell), \tag{17}$$

$$\hat{\theta}_{B,k+1}^{\ell,-} = \hat{\theta}_{B,k}^\ell - \omega_k^e. \tag{18}$$

where u_k^e and ω_k^e depend on the encoder readings $u_{R,k}^e$ and $u_{L,k}^e$ as reported in Section II. Compute the covariance matrix of the obtained estimates:

$$P_{k+1}^{\ell,-} = F_k^\ell P_k^\ell (F_k^\ell)^T + W_k^\ell Q_k (W_k^\ell)^T, \tag{19}$$

where F_k^ℓ and W_k^ℓ are, respectively, the 3×3 and 3×2 Jacobian matrices of the state dynamics with respect to the state and to the encoder noise, while the encoder reading noise covariance matrix Q_k is given by:

$$Q_k = \begin{bmatrix} K_R |u_{R,k}^e| & 0 \\ 0 & K_L |u_{L,k}^e| \end{bmatrix}. \tag{20}$$

Correction step. Also the Correction step is applied independently in each EKF instance ℓ. Let Φ_{k+1} be the vector of the three phase measurements $\phi_{i,k+1}$, $i = 1, 2, 3$, coming from the three antennas in the TLT at time step $k+1$. The expected measurement vector $\hat{\Phi}_{k+1}^\ell$ comprises the three expected phase measurements $\hat{\phi}_{i,k+1}^\ell = \mod(-2KD_{i,k+1}^\ell)$, $i = 1, 2, 3$, with $D_{i,k+1}^\ell$ given by (9), (10) and (11), where all variables in these equations are replaced with their estimates $\hat{\rho}_{k+1}^{\ell,-}$, $\hat{\beta}_{k+1}^{\ell,-}$ and $\hat{\theta}_{B,k+1}^{\ell,-}$. Hence the correction step of the filter is given by:

$$\begin{bmatrix} \hat{\rho}_{k+1}^\ell \\ \hat{\beta}_{k+1}^\ell \\ \hat{\theta}_{B,k+1}^\ell \end{bmatrix} = \begin{bmatrix} \hat{\rho}_{k+1}^{\ell,-} \\ \hat{\beta}_{k+1}^{\ell,-} \\ \hat{\theta}_{B,k+1}^{\ell,-} \end{bmatrix} + K_{k+1}^\ell (\Phi_{k+1} - \hat{\Phi}_{k+1}^\ell), \tag{21}$$

where

$$K_{k+1}^\ell = P_{k+1}^{\ell,-} (H_{k+1}^\ell)^T \left(H_{k+1}^\ell P_{k+1}^{\ell,-} (H_{k+1}^\ell)^T + R_s \right)^{-1} \tag{22}$$

is the 3×3 Kalman gain, H_{k+1}^ℓ is the 3×3 Jacobian matrix of the measurement with respect to the state and $R_s = \sigma_\phi^2 \cdot I_3$ (with I_3 the 3×3 identity matrix) is the covariance matrix of the measurement noise. The covariance matrix is finally updated as follows:

$$P_{k+1}^\ell = (I_3 - K_{k+1}^\ell H_{k+1}^\ell) P_{k+1}^{\ell,-}. \tag{23}$$

Weighing step. The different EKF instances are weighed following the same procedure described in [21], which takes into account the agreement between the true and expected phase measurements coming from the three antennas of the TLT. Instances with a too small weight or with a range estimate larger than $1.1\rho_M$ are moved to cycles corresponding to the current phase measurement not covered by other instances (see always [21] for more details). Take as final estimates of ρ_k and β_k the ones provided by the best EKF instance (i.e. by the EKF instance with the largest weight). □

B. The EKF-SLAM

The range and the bearing estimates of the observed TLT can be used in a simultaneous localization and mapping algorithm, where the data association is available, thanks to the knowledge of the ID of the responding tags. The SLAM algorithm adopted in this paper is based on an Extended Kalman Filter. The robot pose at time k is

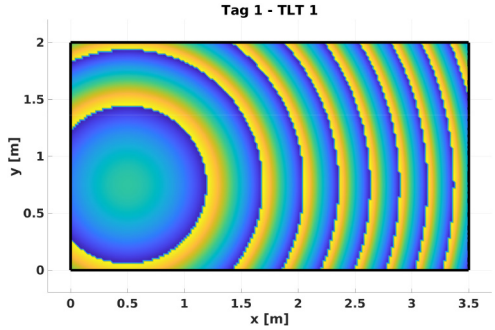

Fig. 4. Ideal phases for tag 1, TLT 1 in the corridor environment.

$(x_{r,k}, y_{r,k}, \theta_k)$, so the state vector, also including the tag coordinates, is a $2L + 3$ dimensional vector given by $x_k = [x_{r,k}, y_{r,k}, \theta_k, x_{T_1,k}, y_{T_1,k}, \ldots, x_{T_L,k}, y_{T_L,k}]^T$. The coordinates $(x_{T_i,k}, y_{T_i,k})$, $i = 1, \ldots, L$, refer to the point P_1 of the i-th TLT, as reported in Section III-A. The dynamics of the system can be written as

$$x_{k+1} = f\left(x_k, u_k^e, w_k^e, n_{R,k}, n_{L,k}\right), \tag{24}$$

which contains $2L+3$ equations, where the first three equations are the robot dynamics (1), while the other $2L$ equations are the constant dynamics of the tag coordinates, i.e., $x_{T_i,k+1} = x_{T_i,k}$ and $y_{T_i,k+1} = y_{T_i,k}$ for all $i = 1, 2, \ldots, L$.

When a new range and bearing measurement with the robot in state $(x_{r,k}, y_{r,k}, \theta_k)$ and the TLT in position $(x_{T_i,k}, y_{T_i,k})$ is available, it can be expressed as follows:

$$h_i(x_k) = \begin{bmatrix} \sqrt{\left(x_{r,k} - x_{T_i,k}\right)^2 + \left(y_{r,k} - y_{T_i,k}\right)^2} \\ \text{atan2}\left(y_{T_i,k} - y_{r,k}, x_{T_i,k} - x_{r,k}\right) - \theta_k \end{bmatrix}. \tag{25}$$

When measurements from L TLTs are available, (25) becomes a function $h(\cdot)$ whose $2L$ elements contain the range and the bearing from the L TLTs. The detailed steps of the EKF-SLAM are reported in Algorithm 2.

IV. Numerical Investigation and Examples

The simulated environment is a 3.5×2 m^2 indoor corridor with two TLTs located on the ceiling: the three antennas of the first TLT are in $(0.5, 0.75)$, $(0.56, 0.85)$, $(0.62, 0.75)$ m, the three antennas of the second TLT in $(2.5, 0.75)$, $(2.56, 0.85)$, $(2.62, 0.75)$. The robot performs random paths that are generated by randomly selecting the initial position and orientation of the robot. When going straight, in each time step the robot covers a distance of about one cm. When performing a turn, the robot covers about 5° per time step. The duration T of the simulations considered in this section is 2000 steps, corresponding to an average of about 15 m of traveled distance. The parameters of the robot are $d = 26$ cm and $K_R = K_L = 0.01$cm. The maximum detection range on the floor is $\rho_M = 150$ cm, and the height of the ceiling with respect to the reader is $h = 255$ cm. The standard deviation σ_ϕ of the noise in the phase measurements is assumed 10°.

A set of 100 simulations has been run with the proposed approach and the performance is measured as in [19], by defining an average robot position estimation error over the last 1000 steps of the simulation

$$e_r = \frac{1}{L}\sum_{i=1}^{L}\left[\frac{1}{1000}\sum_{k=T-999}^{T}|e_{ri,k}|\right], \tag{27}$$

where $e_{ri,k}$ is the difference at time step k between the true and the estimated distance of the robot with respect to TLT i, $i = 1, 2, \ldots, L$, and a map estimation error at the end of the simulation

$$e_t = \frac{1}{L(L-1)/2}\sum_{i=1}^{L-1}\sum_{j=i+1}^{L}\left|e_{tij,T}\right|, \tag{28}$$

where $e_{tij,T}$, $i = 1, 2, \ldots, L-1$ and $j = i+1, \ldots, L$, is the difference at the final time step T between the true and the estimated distance of TLT i with respect to TLT j ($L(L-1)/2$ is the total number of these distances).

The considered scenario is a corridor where along the side walls there are wooden cabinets 0.5 m wide and 2.5 m high

Algorithm 2 The EKF-SLAM With TLT Selection

Initialization. Let $\hat{\rho}_{T_i,0}, \hat{\beta}_{T_i,0}$ be the range and the bearing estimate of the i^{th} TLT at time 0. Assign to (0, 0, 0) the initial robot pose estimate $(\hat{x}_{r,0}, \hat{y}_{r,0}, \hat{\theta}_0)$, i.e. adopt as inertial frame the one with the origin in the initial robot position with the x axis in the initial robot direction. Then, the estimate of the TLT coordinates is initialized as follows: $\hat{x}_{T_i,0} = \hat{\rho}_{T_i,0}\cos(\hat{\theta}_0 + \hat{\beta}_{T_i,0})$ and $\hat{y}_{T_i,0} = \hat{\rho}_{T_i,0}\sin(\hat{\theta}_0 + \hat{\beta}_{T_i,0})$ for all $i = 1, 2, \ldots, L$. Let $k = 0$. Initialize the $(3 + 2L) \times (3 + 2L)$ covariance matrix P_k of the estimates as a block diagonal matrix. The first 3×3 block of P_0 referring to the robot pose is a null matrix, since, by definition, for the choice of the inertial frame, the initial robot pose is exactly known. The other L blocks are 2×2 matrices $P_{0,T_i} = F_{T_i,0} P_{\rho_{T_i,0},\beta_{T_i,0}} F_{T_i,0}^T$, where $F_{T_i,0}$ is the Jacobian matrix of $x_{T_i,0}$ and $y_{T_i,0}$ with respect to $\rho_{T_i,0}$ and $\beta_{T_i,0}$ and $P_{\rho_{T_i,0},\beta_{T_i,0}}$ is the 2×2 submatrix of P_0^ℓ in (15) corresponding to the range and the bearing components (i.e. $P_{\rho_{T_i,0},\beta_{T_i,0}}$ is obtained by taking from P_0^ℓ the first two rows and the first two columns).

Prediction step. At time step k, compute the a priori estimates $\hat{x}_{k+1}^- = f(\hat{x}_k, u_k^e, w_k^e, 0, 0)$, where $f(\cdot)$ has been defined in (24). Compute the covariance matrix of the obtained estimates: $P_{k+1}^- = F_k P_k F_k^T + W_k Q_k W_k^T$, where F_k and W_k are, respectively, the Jacobian matrices of the state dynamics with respect to the state and to the encoder noise and Q_k has been defined in (20).

Correction step. Let z_{k+1} be the $2L$-dimensional vector composed by L couples $[\hat{\rho}_{T_i,k+1}, \hat{\beta}_{T_i,k+1}]$, each one representing the range and the bearing of TLT i with respect to the robot, $i = 1, 2, \ldots, L$, provided by the MHEKF associated with TLT i. The expected value at this stage for this vector is $\hat{z}_{k+1}^- = h(\hat{x}_{k+1}^-)$. Hence the correction step of the filter is given by:

$$\hat{x}_{k+1} = \hat{x}_{k+1}^- + K_{k+1}\left(z_{k+1} - \hat{z}_{k+1}^-\right),$$

where $K_{k+1} = P_{k+1}^- H_{k+1}^T \left(H_{k+1} P_{k+1}^- H_{k+1}^T + R_{k+1}\right)^{-1}$ is the Kalman gain, with H_{k+1} the Jacobian matrix of function $h(\cdot)$ with respect to the state and R_{k+1} the $2L \times 2L$ measurement model covariance matrix: this is a block-diagonal matrix with L blocks given by $P_{\rho_{T_i,k+1},\beta_{T_i,k+1}}$, $i = 1, 2, \ldots, L$, which are the 2×2 submatrices corresponding to the range and bearing components of the covariance matrices $P_{k+1}^{\ell^*}$ computed in (23), related to the EKF selected instance ℓ^* of the MHEKF for TLT i at step $k+1$. The Kalman gain is then modified to only consider the measurements (i.e. range and bearing) coming from TLTs with a *stable* estimate. A TLT estimate is considered stable if the MHEKF is selecting the same EKF instance in the last N consecutive steps, where N is an integer to be properly tuned ($N = 25$ in our implementation). Hence the Kalman gain entries corresponding to a TLT with an unstable estimate are assigned to zero. The covariance matrix is finally updated as follows:

$$P_{k+1} = (I - K_{k+1} H_{k+1}) P_{k+1}^-, \tag{26}$$

with I the $(3 + 2L) \times (3 + 2L)$ identity matrix. □

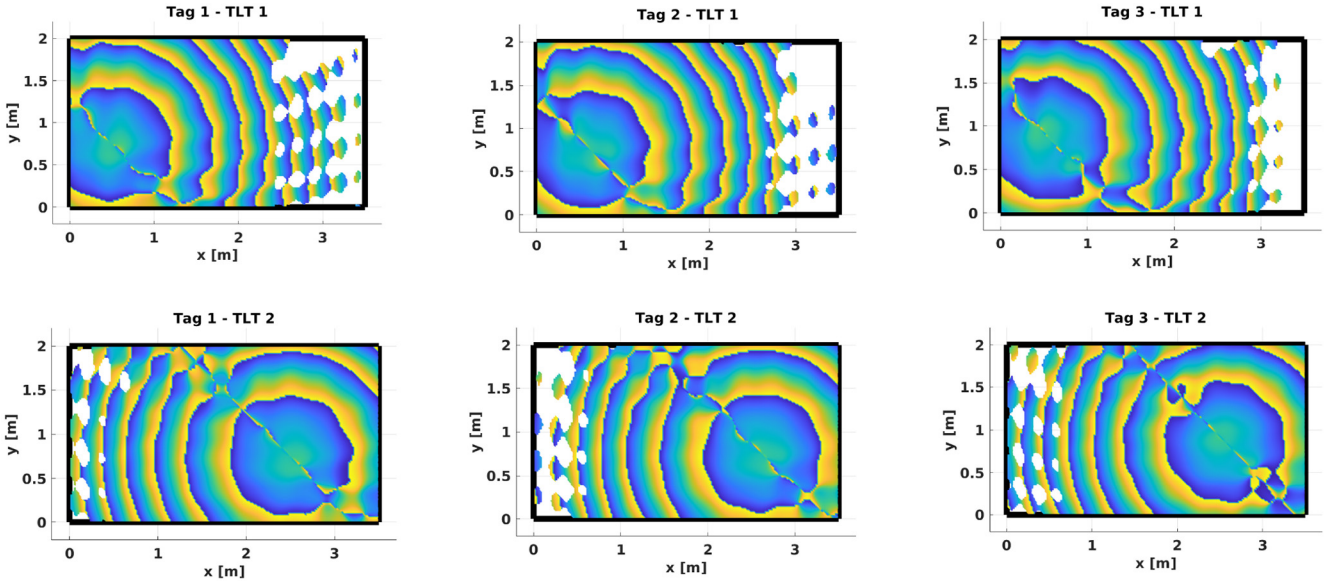

Fig. 5. Multipath affected phases for the 2 TLTs in the corridor environment. The upper figures show the phases for the 3 tags composing TLT 1, while the lower figures show the phases for the 3 tags composing TLT 2.

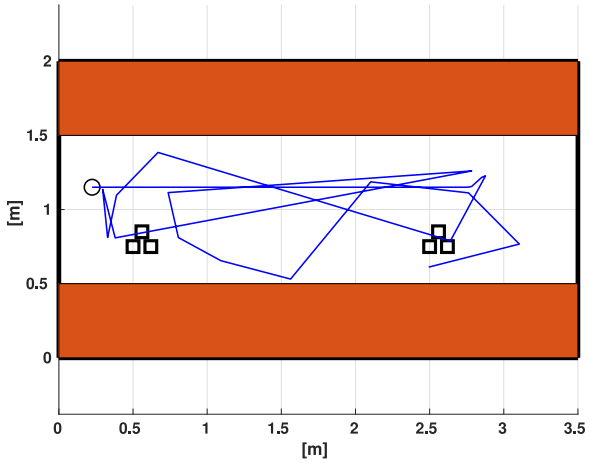

Fig. 6. Layout of the environment where the robot is allowed to move during the simulations. The clustered black squares represent the two TLTs, while the brown rectangles represent the wooden cabinets. A random robot trajectory is depicted in blue (the circle represents the robot initial position).

and long so that they almost entirely cover the walls. The electromagnetic analysis takes into consideration the model of the antennas used and operates with a ray-tracing ([23], [24]) accounting for the direct ray and the first reflection. Evidently the multipath contribution can be considered moderate.

The map (variation) of the phase of the signal received by the robot is shown in Fig. 4, assuming that the tag and the robot were in free space. On the other hand, Fig. 5 shows the maps of the phases of each element of the two TLTs received by the robot antenna within the corridor scenario. From the comparison between the map of Fig. 4 and those of Fig. 5 the effect of the multipath is evident, the equiphase lines lose their regularity while some areas (in white) are not reached by a signal having sufficient intensity to be received because of the destructive interference of multipath.

TABLE I
AVERAGE ROBOT POSITION AND MAP ESTIMATION ERRORS (e_r AND e_t) FOR THE SIMULATIONS ON A FREE SPACE AND MULTIPATH AFFECTED ENVIRONMENTS

Environment type	Average e_r [cm]	Average e_t [cm]
Free space	0.133	1
Multipath affected	0.503	4.346

Fig. 6 shows the layout of the environment with the 2 TLT and the wooden cabinets. The figure also shows the real robot trajectory that has to be estimated by the presented algorithm, together with the position of the TLTs. Table I shows the robot position and map average estimation errors for 100 simulations that have been run in a free space and multipath affected environment. Figs. 7 and 8 show the comparison between the estimation errors on robot position e_r and, respectively, the map estimation errors e_t in a free space environment and space affected by multipath. The results show that the error for the robot position estimation is small (< 1 cm) in both the environments. The map estimation errors are an order of magnitude larger than those of the robot position, but still small and less than 5 cm.

The previous results, for the free space environment, have been also compared to those obtained in [20] where 4 single antenna tags were located in the ceiling of a 2×2 m^2 free space environment. The results of the simulations for the two algorithms are depicted in Fig. 9. The average e_r for 100 simulations ran in [20] is 0.93 cm that, compared with the one obtained from the presented method, shows a reduction of 85.7%, whilst for the average e_t, which was 1.44 cm, a reduction of 30.6%.

V. EXPERIMENTAL RESULTS

A set of experimental tests has been performed in the office room depicted in Fig. 10. The robot used in the experiments

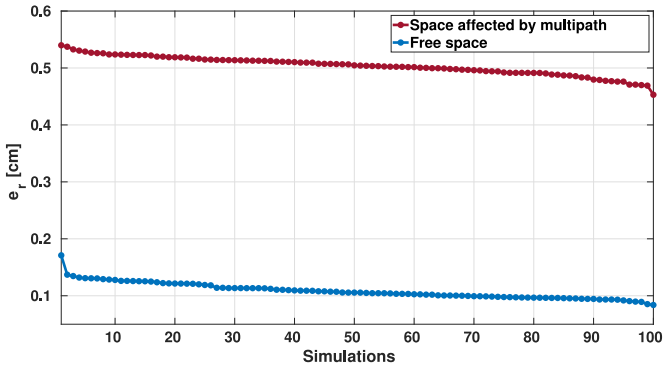

Fig. 7. Comparison between estimation errors on robot position e_r, for the presented SLAM method. The blue diagram depicts the errors over 100 simulations in free space, while the red diagram shows the errors in space affected by multipath.

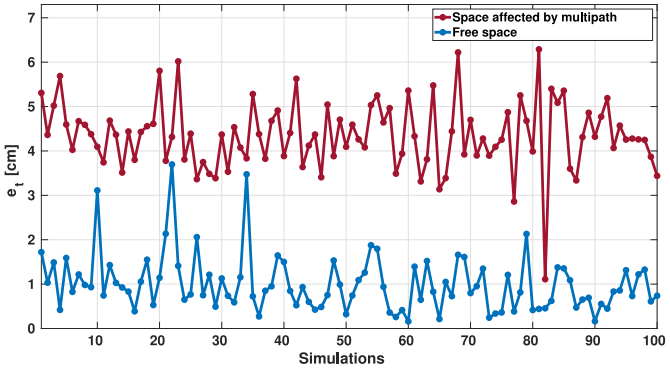

Fig. 8. Comparison between map estimation errors at the end of the simulation e_t, for the presented SLAM method. The blue diagram depicts the errors over 100 simulations in free space, while the red diagram shows the errors in space affected by multipath.

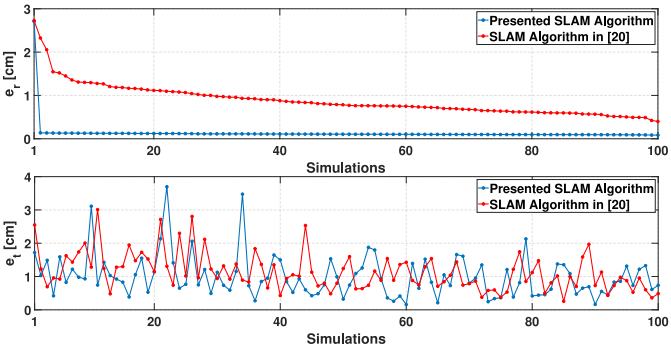

Fig. 9. Comparison between errors e_r and e_t for the presented method (blue) and the SLAM method presented in [20] (red).

(see Fig. 11) is a custom unicycle-like vehicle with a differential drive kinematics, where the distance between the left and the right wheel is 38.2 cm. The robot mounts a Raspberry Pi 4 with a Linux Ubuntu 20.04 OS where a motion planner has been developed for the high level control. An Arduino Mini is also installed in order to control the low level references to the motors and the encoder readings. The reader antenna is placed on board the robot at a height of 35 cm from the floor, it is a right-hand circularly polarized microstrip patch antenna with 7 dBi of gain. The reader (M6e ThingMagic),

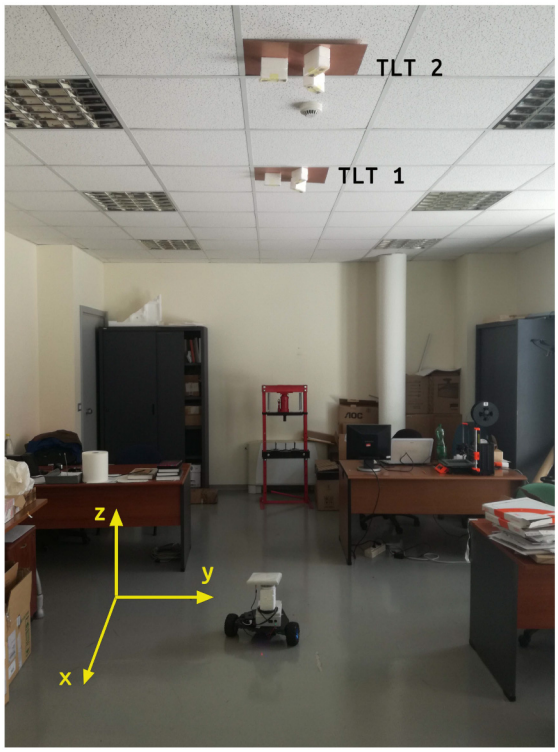

Fig. 10. The experimental setup, with the two TLTs on the ceiling and the robot during its mission. The (x, y, z) frame selected according to the initial pose of the robot is also reported.

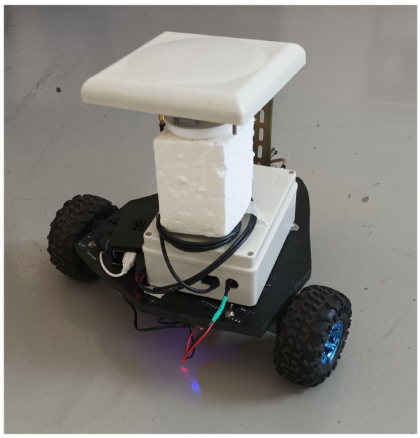

Fig. 11. The robot used in the experiments. The UHF-RFID antenna is mounted on top of the robot.

wireless controlled by means of a remote PC and a Raspberry Pi 4 on board the robot, supplies the antenna with a power of 25 dBm and collects measured data with a rate of 15 Hz while the robot moves with a speed of 0.2 m/s. Measurements have been performed at the frequency of 867 MHz.

Two TLT tags have been deployed on the ceiling of an office room at distance of 1.5 m, as shown in Fig. 10. They are composed of three in-lay tags, with mutual distances L_{ij} of about 17.5 cm, placed radially with angle of 120° over a copper ground plane. Each in-lay tag (LAB-ID UH107) is attached over a substrate of polystyrene foam having thickness 8 cm, as shown in Fig. 12. The thickness of the foam is about a quarter

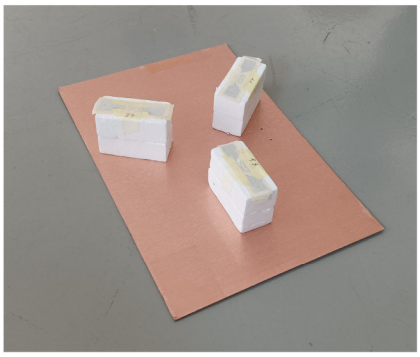

Fig. 12. The TLT used in the experiments. The three in-lay tags are placed radially with an angle of 120°, mounted over a polystyrene substrate, resting on a copper surface.

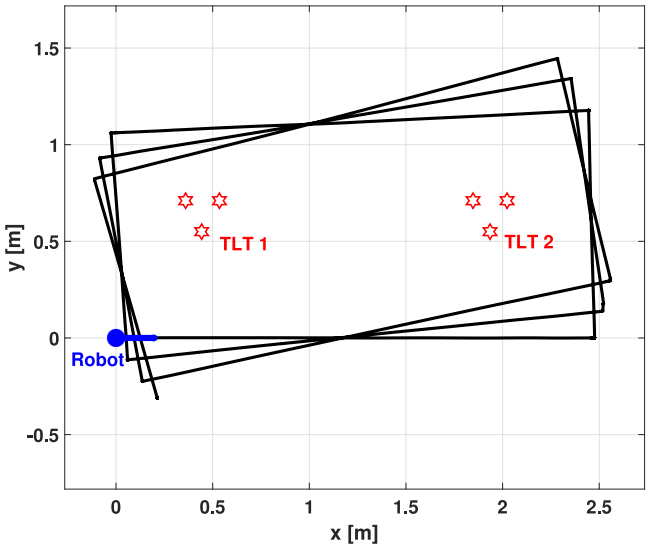

Fig. 13. A map of the considered environment, with the robot in its initial position and orientation (defining the global frame adopted) and the (x, y) position of the two TLTs considered in the experiment. The path estimated by applying the proposed SLAM algorithm is also reported.

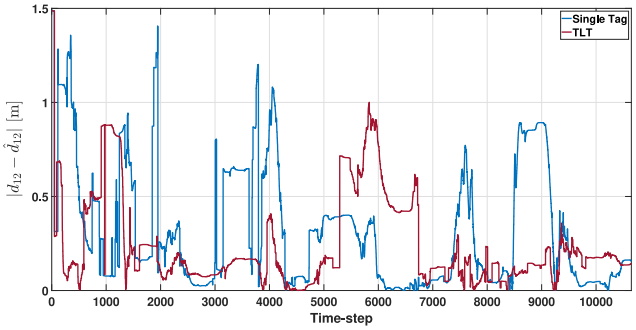

Fig. 14. The figure shows the estimation error on the distance between the two tags during the run for the single tag setup (in blue) and for the TLT (in red) using only the MHEKF with the robot odometry.

of wavelength in order to preserve the radiation capability and the impedance matching of the in-lay tag when placed over the metallic ground plane. The distance between the plane of placement of the tags and the plane of placement of the reader antenna is about 2.5 m.

The experiments have been conducted with the robot moving autonomously along a rectangular path while collecting data from the encoders and from the UHF-RFID reader. The data collected during the runs have been used offline to feed the developed algorithms and to assess their performances. A map of the environment is reported in Fig. 13 together with the estimated robot trajectory for the experiment described in this section. Nominally the robot is requested to cover a rectangular path performing three turns in the area under the tags. The requested trajectory is followed open loop by the robot. Due to several kinds of disturbance, the actual trajectory was quite different from the nominal rectangular one, as witnessed by the trajectory reconstructed by the SLAM algorithm. The ground truth of the overall trajectory is not available in this experiment: we only measured the final position of the robot at the end of its mission, which allowed to compute the performance indexes considered in this paper. In particular, we report in Tables II and III the true and the estimated distances d_{12} between the two tags and, respectively, the true and the estimated distance d_i of the final robot position from the projection on the floor of the two tags ($i = 1, 2$) in the case of the TLTs and in the case of the Single antenna Tags (ST) considered in [20]. In the ST case the tags in position $(0.36, 0.71)$ and $(1.85, 0.71)$ have been considered. From the tables, it can be observed how the use of the TLTs in place of single antenna tags allows to obtain a slight improvement in the performance of the algorithm.

The main reason of the better performance is that the estimate of the tag position when considering TLTs in place of single antenna tags becomes noticeably more reliable. This is essentially due to the availability of three phase measurements for each tag in place of just one. This is illustrated in Fig. 14, where it is possible to observe how the distance between the estimated position of the two TLTs during the experiment presents a faster convergence rate and is in general more frequently close to its true value with respect to the case where two single antenna tags were considered. From Fig. 14 it is possible to observe how in the case of TLTs, the estimation error is usually smaller than 20 cm apart from the time interval around time-step 6000: this depends on the selection in that interval of a bad MHEKF instance, possibly due to multipath effects or to other unmodeled disturbances. This bad behavior of the MHEKF however does not significantly affect the solution to the SLAM problem since the main EKF-SLAM algorithm properly handles this situation by ignoring unstable TLT estimates.

The estimation errors in the experimental tests are larger with respect to the ones obtained in the simulation scenario and also the improvement obtained using TLTs in place of single antenna tags is less evident: this is due to several unmodeled phenomena, like multipath effects and the dependence of the phase measurements on the relative tag-reader orientation, which afflict both the situations. The estimation of the offset allows in part to cope with these unmodeled phenomena and to produce an acceptable behavior, which could be further improved by developing a more comprehensive phase measurement model.

TABLE II
INTER-TAG DISTANCE d_{12} (IN CM): TRUE AND ESTIMATED IN CASE OF TLT AND SINGLE ANTENNA TAGS (ST)

true	estimated (TLT)	estimated (ST [20])
149.20	161.41	165.89

TABLE III
DISTANCES (IN CM) OF THE ROBOT FROM THE ESTIMATED TAGS: TRUE AND ESTIMATED IN CASE OF TLT AND SINGLE ANTENNA TAGS (ST)

d_i	true	estimated (TLT)	estimated (ST [20])
d_1	75.98	91.72	93.81
d_2	193.71	179.64	214.33

VI. CONCLUSION

A SLAM problem has been considered in this paper for a mobile robot, equipped with an odometry sensor (encoders) and measuring the phase of the signal backscattered by a set of UHF-RFID passive tags deployed in unknown position on the ceiling of the environment. The paper introduces a particular kind of tag, denoted as TriLateration Tag (TLT), comprising three antennas close one each other, which form a triangular structure with known shape and dimension. A set of Multi-Hypothesis Extended Kalman Filters, one for each TLT, allows to dynamically estimate the range and the bearing of the detected TLT with respect to the robot. These estimates are then used in an EKF-SLAM algorithm solving the SLAM problem. The approach is robust against several kinds of disturbances and improves, also from this point of view, the performance of other methods presented in the literature in this context. If the offset in the measurements is included in the estimation process, the approach does not require any preliminary calibration procedure, apart from an approximate measurement of the ceiling height, where the tags are placed. As future work, the relative orientation of the TLT with respect to the robot, provided by the MHEKF in addition to the range and the bearing of the TLT, could be included in the SLAM algorithm and would allow in principle to solve the SLAM problem even if only one TLT is available in the environment.

REFERENCES

[1] A. Motroni, A. Buffi, and P. Nepa, "A survey on indoor vehicle localization through RFID technology," *IEEE Access*, vol. 9, pp. 17921–17942, 2021.

[2] C. Zhou and J. D. Griffin, "Accurate phase-based ranging measurements for backscatter RFID tags," *IEEE Antennas Wireless Propag. Lett.*, vol. 11, pp. 152–155, 2012.

[3] Y. Ma, N. Selby, and F. Adib, "Minding the billions: Ultra-wideband localization for deployed RFID tags," in *Proc. 23rd Annu. Int. Conf. Mobile Comput. Netw. (ACM MobiCom)*, Oct. 2017, pp. 248–260.

[4] R. Miesen, F. Kirsch, and M. Vossiek, "UHF RFID localization based on synthetic apertures," *IEEE Trans. Autom. Sci. Eng.*, vol. 10, no. 3, pp. 807–815, Jul. 2013.

[5] A. Tzitzis *et al.*, "Trajectory planning of a moving robot empowers 3D localization of RFID tags with a single antenna," *IEEE J. Radio Freq. Identificat.*, vol. 4, no. 4, pp. 283–299, Dec. 2020.

[6] H. Wu, B. Tao, Z. Gong, Z. Yin, and H. Ding, "A fast UHF RFID localization method using unwrapped phase-position model," *IEEE Trans. Autom. Sci. Eng.*, vol. 16, no. 4, pp. 1698–1707, Oct. 2019.

[7] E. Di Giampaolo and F. Martinelli, "Mobile robot localization using the phase of passive UHF RFID signals," *IEEE Trans. Ind. Electron.*, vol. 61, no. 1, pp. 365–376, Jan. 2014.

[8] A. Motroni, A. Buffi, P. Nepa, and B. Tellini, "Sensor-fusion and tracking method for indoor vehicles with low-density UHF-RFID tags," *IEEE Trans. Instrum. Meas.*, vol. 70, pp. 1–14, 2021.

[9] B. Tao, H. Wu, Z. Gong, Z. Yin, and H. Ding, "An RFID-based mobile robot localization method combining phase difference and readability," *IEEE Trans. Autom. Sci. Eng.*, vol. 18, no. 3, pp. 1406–1416, Jul. 2021.

[10] V. Magnago *et al.*, "Ranging-free UHF-RFID robot positioning through phase measurements of passive tags," *IEEE Trans. Instrum. Meas.*, vol. 69, no. 5, pp. 2408–2418, May 2020.

[11] A. Buffi *et al.*, "UHF-RFID localization: The problem of antenna phase center in phase-based methods," in *Proc. 13th Conf. Antennas Propag. EuCAP*, Krakow, Poland, Apr. 2019, pp. 1–5.

[12] F. Martinelli, "A robot localization system combining RSSI and phase shift in UHF-RFID signals," *IEEE Trans. Control Syst. Technol.*, vol. 23, no. 5, pp. 1782–1796, Sep. 2015.

[13] F. Martinelli, "Robot localization using the phase of passive UHF-RFID signals under uncertain tag coordinates," *J. Intell. Robot. Syst.*, vol. 82, pp. 577–593, Jun. 2016.

[14] D. Joho, C. Plagemann, and W. Burgard, "Modeling RFID signal strength and tag detection for localization and mapping," in *Proc. Conf. Robot. Autom. ICRA*, 2009, pp. 12–17.

[15] J. Djugash, S. Singh, and P. I. Corke, "Further results with localization and mapping using range from radio," in *Proc. Int. Conf. Field Service Robot. (FSR)*, Jul. 2005, pp. 231–242.

[16] E. Giannelos, E. Andrianakis, K. Skyvalakis, A. G. Dimitriou, and A. Bletsas, "Robust RFID localization in multipath with phase-based particle filtering and a mobile robot," *IEEE J. Radio Freq. Identificat.*, vol. 5, no. 3, pp. 302–310, Sep. 2021.

[17] F. Martinelli, "Simultaneous localization and mapping using the phase of passive UHF-RFID signals," *J. Intell. Robot. Syst.*, vol. 94, pp. 711–725, Jun. 2019.

[18] J.-L. Blanco, J. Fernandez-Madrigal, and J. Gonzalez, "Efficient probabilistic range-only SLAM," in *Proc. IEEE/RSJ Int. Conf. Intell. Robots Syst.*, 2008, pp. 1017–1022.

[19] E. Di Giampaolo and F. Martinelli, "A restarting paradigm for a range-only SLAM algorithm using the phase of passive UHF-RFID signals," in *Proc. IEEE RFID-TA*, Sep. 2019, pp. 24–27.

[20] F. Martinelli and F. Romanelli, "A SLAM algorithm based on range and bearing estimation of passive UHF-RFID tags," in *Proc. 11th IEEE Int. Conf. RFID Technol. Appl. (IEEE RFID-TA)*, Oct. 2021, pp. 6–8.

[21] E. Di Giampaolo and F. Martinelli, "Range and bearing estimation of an UHF-RFID tag using the phase of the backscattered signal," *IEEE J. Radio Freq. Identificat.*, vol. 4, no. 4, pp. 332–342, Dec. 2020.

[22] E. Di Giampaolo, F. Martinelli, and F. Romanelli, "A localization system for autonomous vehicles based on TriLateration tags," in *Proc. 16th Eur. Conf. Antennas Propagat. (EuCAP)*, Mar. 2022, pp. 1–5.

[23] E. Di Giampaolo and F. Bardati, "Analytical model of multiple wedge-diffracted ray congruence," *Electromagnetics*, vol. 23, no. 6, pp. 509–523, 2003.

[24] E. Di Giampaolo and F. Bardati, "A projective approach to electromagnetic propagation in complex environments," *Progr. Electromagn. Res. B*, vol. 13, pp. 357–383, Mar. 2009.

Emidio Di Giampaolo received the Laurea degree in electronic engineering and the Ph.D. degree in applied electromagnetics from the University of L'Aquila, Italy, in 1994 and 1998, respectively.

From 1998 to 2004, he was a Postdoctoral Researcher with the University of L'Aquila. In Spring 2000, he was a Visiting Researcher with the European Space Research and Technology Centre, Noordwijk, The Netherlands. From 2005 to 2009, he was a Researcher with the University of Rome Tor Vergata. Since 2010, he has been with the University of L'Aquila as an Associate Professor. His research interests mainly concern numerical methods for modeling radio-wave propagation in complex environments, antennas, and radio localization.

Francesco Martinelli was born in Rome, Italy, in 1969. He received the Laurea degree (*cum laude*) in electrical engineering and the Ph.D. degree in computer science and automation engineering from the University of Rome Tor Vergata, Italy, in 1994 and 1998, respectively.

He is currently an Associate Professor with the University of Rome Tor Vergata. In 1997, he was a Visiting Scholar with the Department of Manufacturing Engineering, Boston University, Boston, MA, USA. His research interests include mobile robot localization, dynamic scheduling of manufacturing systems, and filtering methods.

Fabrizio Romanelli was born in Viterbo, Italy, in 1979. He received the B.S. and M.S. degrees in automation engineering from the University of Rome Tor Vergata in 2005, where he is currently pursuing the Ph.D. degree in computer science, control, and geoinformation, focusing on robotic perception and sensor fusion techniques.

From 2006 to 2017, he was a Robotics Specialist and a Software Manager with the Research and Development Department, Comau Robotics S.p.A., Turin, Italy. From 2017 to 2019, he was a Research Engineer with the Istituto Italiano di Tecnologia, Genoa, Italy, in the Advanced Robotics Research Line designing the software architecture for legged robots. He is the author of 14 articles and one book chapter. He holds two patents. His research interests include resilient robotic perception, sensor fusion techniques, simultaneous localization and mapping, visual SLAM, and plasma magnetic control in Tokamak devices.

Mr. Romanelli was a finalist at the EUROP/EURON Technology Transfer Award 2009 and won the Second Prize at the EUnited Robotics Technology Award 2014.

Open Access funding provided by 'Università degli Studi di Roma "Tor Vergata"' within the CRUI CARE Agreement